Viscous modes within the compressible boundary-layer flow due a broad rotating cone

P.D. TOWERS
Department of Mathematics, University of Leicester

Z. HUSSAIN
School of Computing, Mathematics & Digital Technology, Manc. Met. University

P.T. GRIFFITHS
Department of Engineering, University of Leicester

AND

S.J. GARRETT
Department of Engineering, University of Leicester

We investigate the effects of compressibility on the stationary, viscous (Type II) instability mode within the three-dimensional boundary layer over rotating cones with half-angle greater than 40°. The stationary mode is characterised by zero shear stress at the wall and a triple-deck solution is presented in the isothermal case. Asymptotic solutions are obtained which describe the structure of the wavenumber and the orientation of this mode as a function of local Mach number. It is found that a stationary mode is possible only over a finite range of local Mach number. Our conclusions are entirely consistent with the results of Seddougui [*Q. Jl Mech. appl. Math.* **43**]. It is suggested that wall-cooling has a significant stabilising effect, while reducing the half-angle is marginally destabilising. All numerical results are presented for air.

Keywords: rotating cone, Type II, compressible boundary-layer flow

1. Introduction

The study of the boundary-layer flow due to a rotating disk has been the subject of great interest for many decades. This enduring interest is predominately motivated by the disk's fundamental importance as a model for cross-flow dominated flows, such as those that appear over swept wings and in other applications. Despite a consistent focus on the disk since the 1950s, only during the past couple of decades has interest increased into the boundary-layer flows over other axisymmetric rotating bodies. Engineering advances related to spinning projectiles and aeroengine components, for example, have now led to the study of flows over rotating hemispheres and cones as being of direct industrial importance. A better understanding of the onset of laminar-turbulent transition over these more exotic geometries could therefore potentially lead to improved engineering designs in a number of industrial sectors.

From the very early work of Gregory *et al.* (1955) and Gregory & Walker (1960) through to Hall (1986), Malik (1986), Lingwood (1995, 1996) and beyond to the very recent studies of Imayama *et al.* (2013), Appelquist (2014), Griffiths (2015) and Cooper *et al.* (2015), the flow over the rotating disk has been studied extensively in the case of *incompressible* flows. Similarly, experimental work by Kappesser *et al.* (1973) and Kobayashi and co-workers (Kobayashi 1981; Kobayashi *et al.* 1983; Kobayashi &

Izumi 1983), for example, has led to the more recent theoretical studies of Garrett, Hussain and co-workers (Garrett & Peake 2007; Garrett *et al.* 2009; Hussain *et al.* 2014, 2015), who have made progress in understanding the stability characteristics of the incompressible flow over the family of rotating cones. However, despite Seddougui (1990) and Turkyilmazoglu and co-workers (Turkyilmazoglu *et al.* 2000; Turkyilmazoglu & Uygun 2004; Turkyilmazoglu 2005, 2007) making significant progress in the study of the *compressible* disk flow, there has been little work investigating the compressible cone flow.

The rotating-disk flow is clearly a special case of the rotating-cone flow with half-angle, ψ, set to 90°. Studies of the rotating-cone flow can therefore be thought of as a generalisation of the significant body of work on the rotating disk. The motivation for this current study is to generalise the work of Seddougui (1990) from the compressible disk flow to the compressible cone flow, thereby extending the previous work on the incompressible cone flow due to Garrett *et al.* (2009) The study is intended as a step towards advances in the aforementioned engineering applications. In particular, understanding the instability mechanisms of the rotating-cone flow could enable the control of laminar-turbulent transition within the boundary layer, which may lead to performance improvements in high-speed applications, potentially through the use of surface cooling or mass flux. For spinning projectiles, for example, a transition delay could help reduce drag as well as having beneficial effects on control and targeting. Furthermore, in aeroengine components, advances could help fuel efficiency by enabling the careful control of inlet flows or reducing drag.

The body of work on rotating cones (including the disk) has demonstrated that the initial onset of laminar-turbulent transition is dominated by two instability modes, typically referred to as the Type I and Type II modes. The Type I mode is inviscid in nature and due to the well-known crossflow instability (see for example Malik 1986; Lingwood 1995; Garrett *et al.* 2009; Cooper *et al.* 2015 and references contained therein). In contrast, the Type II mode is viscous in nature and attributed to external streamline curvature (Itoh 1994, 1996). The more recent work of Garrett, Hussain & Stephen (Hussain *et al.* 2014, 2015) has, however, identified the existence of a third convective mode that arises from centrifugal effects. We note that this mode is important only over slender cones and, in this current analysis of *broad* cones, is not relevant. The distinction between "slender" and "broad" is expected to be $\psi \approx 40^\circ$, and we are concerned here with $\psi > 40^\circ$.

A preliminary, leading-order analysis of the inviscid (Type I) mode of the compressible rotating-cone flow has been given by Towers & Garrett (2012) and in this current paper we present a full analysis of the viscous (Type II) mode. We begin, in §2., by formulating the problem and summarising the derivation of the steady flow. The computation of the steady flow is significantly complicated by the introduction of compressibility and the full detailed calculations are presented elsewhere by Towers & Garrett (2014). The governing, linearized perturbation equations are then derived in §3. and we proceed with a triple-deck analysis of disturbances that rotate with the surface of the cone (i.e. stationary modes). The results are discussed in §4. and our conclusions are drawn in §5.. Note that, although our presentation of the analysis is given for a cone rotating in a general gas, any numerical results are presented in the particular case of air.

2. Steady flow

A detailed derivation of the relevant steady flows has been published separately by Towers & Garrett (2014) and the interested reader is referred there for full details. Here we summarise that derivation by way of formulating the system for the detailed stability analysis presented in §3..

Consider a cone with rigid, isothermal wall of infinite extent with half-angle ψ rotating with angular velocity Ω^* in an otherwise still, compressible fluid. We choose an orthogonal curvilinear coordinate

system (x^*, θ, z^*) with origin placed at the tip of the cone and rotates with it, consistent with all recent studies of the cone geometry by the current authors (Towers & Garrett 2014; Garrett *et al.* 2009; Hussain *et al.* 2014). The coordinate variables represent the streamwise (i.e. along the cone surface), azimuthal and surface-normal variation, respectively, and the axis of rotation is aligned with the Cartesian X^*-axis such that

$$\begin{aligned} X^* &= x^* \cos\psi - z^* \sin\psi, \\ Y^* &= (x^* \sin\psi + z^* \cos\psi)\sin\theta, \\ Z^* &= (x^* \sin\psi + z^* \cos\psi)\cos\theta. \end{aligned}$$

Here Y^* and Z^* are the other Cartesian axes. The governing Navier–Stokes, state and energy equations in this coordinate system can be found elsewhere (Towers 2013; Towers & Garrett 2014). The local cross-sectional radius at distance x^* along the cone is given by $r^* = x^* \sin\psi$. As was discussed in §1., we restrict our analysis to broad cones and so it is assumed that $\psi > 40^\circ$. The superscript * denotes a dimensional quantity in all that follows.

The system is characterised by the second coefficient of viscosity, λ^*, the dynamic viscosity, μ^*, and enthalpy, h^*. Furthermore, the heat capacity ratio γ is the ratio of the heat capacity at constant pressure, c_{p}^*, to the heat capacity at constant volume, c_{v}^*. We also introduce the parameter k^* that is associated with the Prandtl number σ, where $k^*\sigma = c_{\mathrm{p}}^*\mu^*$. The temperature of the fluid is denoted by T^*, density ρ^*, and pressure p^*. Note that any evaluations will assume that the cone is rotating in air and so $\sigma = 0.7$ and $\gamma = 1.4$.

We introduce a characteristic length scale along the cone surface l^* and non-dimensionize the spatial variables as follows

$$x^* = l^* x, \qquad z^* = l^* x, \qquad z = Re^{\frac{1}{2}}\eta,$$

where Re is the Reynolds number, defined by

$$Re = \frac{\rho^* l^{*2} \Omega^* \sin\psi}{\mu^*}. \tag{2..1}$$

The quantity η is interpreted as the surface-normal spatial variable within the boundary-layer. The velocity quantities are then scaled by

$$\mathbf{u}^* = l^* \Omega^* \sin\psi \big(u(x,\eta), v(x,\eta), Re^{-\frac{1}{2}} w(x,\eta)\big),$$

and the pressure is scaled using

$$p^* = \rho^* \Omega^{*2} l^{*2} \sin^2\psi . p(x,\eta).$$

All other flow parameters are scaled by their free-stream equivalents (indicated by a subscript $_\infty$) and we define the free-stream Mach number in terms of known parameters as

$$M_\infty = \frac{\Omega l}{(\gamma R_{\mathrm{gas}} T_\infty)^{\frac{1}{2}}}, \tag{2..2}$$

with the specific gas constant defined by Mayer's relation, $R_{\mathrm{gas}} = c_{\mathrm{p}} - c_{\mathrm{v}}$.

The governing equations are non-dimensionalised as indicated and all time and θ dependence is neglected to enforce a rotationally symmetric, steady flow. Furthermore, we expand in powers of Re and, following the assumption of large Reynolds number, dismiss all terms $\mathscr{O}(Re^{-\frac{1}{2}})$. Physically, this limits

the analysis to high rotation rates and/or large characteristic length scales relative to the boundary-layer thickness and is entirely appropriate for our intentions. This results in the governing boundary-layer equations as given by Eqs. (9)–(15) of Towers & Garrett (2014) and are subject to the no-slip condition on the cone surface and quiescent/free-stream conditions at the edge of the boundary layer.

Following Towers & Garrett (2014), we assume that the fluid obeys Chapman's viscosity law, that is $\mu = CT$ for some constant C which we set to unity without loss of generality. A Dorotonitsyn–Howarth (Stewartson 1964) transformation is then made to the normal coordinate to remove dependence on the density ρ,

$$y = \int_0^\eta \rho \, \mathrm{d}\eta,$$

and we seek a similarity solution of the form

$$\big(u(x,y), v(x,y), w(x,y), p(x,y)\big) = \big(xU(y), xV(y), W(y), (\gamma M_\infty^2)^{-1}\big). \tag{2..3}$$

Note that the pressure profile, $p(x,y)$, is assumed to be constant. Introducing the stream function, $\Psi(y)$, such that $U = \Psi'(y)$ and $W = -T\left(2\Psi + x\Psi'\frac{\partial y}{\partial x}\right)$ leads to the generalised set of von Kármán equations

$$(\Psi')^2 - 2\Psi\Psi'' - (V+1)^2 = \Psi''', \tag{2..4}$$

$$2(V+1)\Psi' - 2\Psi V' = V'', \tag{2..5}$$

$$\frac{\partial^2 T}{\partial y^2} + 2\sigma\Psi\frac{\partial T}{\partial y} - x\sigma\Psi'\frac{\partial T}{\partial x} + (\gamma-1)\sigma x^2 M_\infty^2\left(\Psi''^2 + v^2\right) = 0, \tag{2..6}$$

where a prime denotes $\frac{\mathrm{d}}{\mathrm{d}y}$. The equations are subject to the boundary conditions

$$\Psi(0) = \Psi'(0) = \Psi(\infty) = V(0) = V(\infty) + 1 = T(\infty) - 1 = 0.$$

Equations (2..4) & (2..5) are coupled ODEs in y and can be solved easily to generate $U(y)$ and $V(y)$; these are found to be identical to the associated components of the standard von Kármán flow. The temperature profile, and therefore $W(y)$, can then be found from Eq. (2..6). Rather than solving this PDE directly, progress is made by introducing the local Mach number

$$M_x = x\sin\psi M_\infty = rM_\infty, \tag{2..7}$$

and imposing the temperature relation originally used by Riley (1964)

$$T(y) = 1 - \frac{\gamma-1}{2}M_x^2 f(y) + (T_w - 1)q(y). \tag{2..8}$$

This enables the PDE to be written as two ODEs in y, specifically

$$f'' + 2\sigma\Psi f' - 2\sigma\Psi' f = \frac{2\sigma\left(\Psi''^2 + V'^2\right)}{\sin^2\psi}, \tag{2..9}$$

$$q'' + 2\sigma\Psi q' = 0. \tag{2..10}$$

The quantity $f(y)$ is interpreted as a viscous dissipation quantity, and $q(y)$ a heat conduction term. These are such that Eqs. (2..9) & (2..10) satisfy the boundary conditions

$$f(0) = f(\infty) = q(0) - 1 = q(\infty) = 0.$$

Equation (2..9) has an exact analytical solution and Eq. (2..10) permits a straightforward numerical solution. A detailed discussion of the flow profiles in terms of transformed spatial variable y is given elsewhere by Towers & Garrett (2014) and Towers (2013).

In the stability analysis that follows we will return to the governing equations expressed in terms of the coordinate system (x,θ,z). It is therefore necessary to express the steady flows in terms of non-dimensional variable z. We invert the Dorodnitsyn–Howarth transformation and find that

$$z=(\sin\psi)^{-\frac{1}{2}}\left(y-\frac{\gamma-1}{2}M_x^2\int_0^y f\,\mathrm{d}y+(T_w-1)\int_0^y q\,\mathrm{d}y\right),$$

which reintroduces several of the flow parameters that had been scaled out.

The resulting steady velocities are discussed elsewhere in Towers & Garrett (2014) and the interested reader is referred to there.

3. Stability analysis

We now proceed to formulate a stability analysis of the steady flows (u,v,w,ρ,T) obtained in §2.. This is done by imposing perturbations on the velocity, pressure, density and temperature fields expressed in terms of the spatial coordinate system (x,θ,z). A local analysis will be conducted at fixed values of the streamwise spatial variable x, that is, at a particular distance along the cone surface. The non-dimensionalising scalings detailed in §2. are also used for the perturbing quantities, with the exception of the normal velocity component which is now assumed to be of the same order as the other velocity components.

The perturbed quantities are substituted into the governing equations and linearised to give the linear perturbation equations stated in Appendix A. Henceforth the perturbing quantities will be denoted $\tilde{u},\tilde{v},\tilde{w},\tilde{p},\tilde{\rho}$ and $\tilde{T}$; that is, the perturbed quantities have the form $u+\tilde{u}$ and similarly for all other quantities. Note that, in general, the perturbing quantities are not forced to be rotationally symmetric or steady and so derivatives $\frac{\partial}{\partial\theta}$ and $\frac{\partial}{\partial t}$ of the perturbing quantities are not necessarily zero. However, here we consider stationary disturbances and so all time dependence is again neglected. The physical interpretation of this in this rotating frame of reference is that disturbances are fixed on the cone surface.

Following the method developed by Smith (1979) for the Blasius boundary-layer, we consider a triple-deck structure for the stationary viscous modes. Our analysis is based on the small parameter

$$\varepsilon=Re^{-\frac{1}{16}}$$

and the upper, main and lower decks are assumed to be of thickness $\mathscr{O}\left(\varepsilon^4\right)$, $\mathscr{O}\left(\varepsilon^8\right)$ and $\mathscr{O}\left(\varepsilon^9\right)$, respectively. Note that the assumption that $\varepsilon<<1$ is consistent with the assumption of high Reynolds number required in the derivation of the steady flow. The upper deck is inviscid and irrotational and creates a pressure gradient to drive the flow into the lower deck. The main deck is also inviscid with no pressure change across the layer. All viscous effects are therefore contained in the lower deck, which has to satisfy the no-slip condition on the surface of the cone. The analysis that follows is consistent with that of Seddougui (1990) who considered the related problem of the compressible rotating-disk boundary layer (i.e. $\psi=90^\circ$).

We seek a normal-mode solution for the stationary perturbing field and impose

$$\tilde{u}(x,\theta,z)=\bar{u}(z)\exp\left(\frac{\mathrm{i}}{\varepsilon^4}\int^x\alpha(x,\varepsilon)\mathrm{d}x+\beta(\varepsilon)\theta\right), \tag{3..1}$$

with similar expressions for $\tilde{v},\tilde{w},\tilde{p},\tilde{\rho}$ and $\tilde{T}$. Here α and β are interpreted as the streamwise and azimuthal wavenumbers and are expanded as

$$\alpha = \alpha_0 + \varepsilon^2\alpha_1 + \varepsilon^3\alpha_2 + \ldots,$$
$$\beta = \beta_0 + \varepsilon^2\beta_1 + \varepsilon^3\beta_2 + \ldots.$$

We restrict our analysis to neutral disturbances and seek to find α and β such that the flow is neutrally stable at position x. That is, we impose that $\alpha,\beta \in \mathbb{R}$.

The analysis that follows is necessarily complicated and it is inappropriate to give full mathematical details here. The interested reader is therefore referred to Towers (2013) for full mathematical detail.

3.1. *Upper-deck solutions*

In the upper deck we define $z = \varepsilon^4 Z$ so that the normal spatial variable Z is $\mathcal{O}(1)$, and expand all perturbing quantities (3..1) with

$$\bar{u} = \varepsilon^3 u_0^U(Z) + \varepsilon^4 u_0^U(Z) + \ldots.$$

Note that the superscript ^{U} is used to denote a quantity in the upper deck. In the upper deck the steady-flow quantities take their free-stream values, that is $u = 0$, $v = -1$, $\rho = 1$, $T = 1$ and p is a constant. Substituting these steady and perturbing quantities into the governing perturbation equations (A.1)–(A.6) leads to modified equations than can be combined in a single ODE for p_0^U

$$\frac{\mathrm{d}^2 p_0^U}{\mathrm{d}Z^2} - \Gamma^2 p_0^U = 0, \tag{3..2}$$

where the leading-order wavenumber, Γ, is defined by

$$\Gamma^2 = \alpha_0^2 + \frac{\beta_0^2}{x^2\sin^2\psi}\left(1 - M_x^2\right).$$

Rejecting solutions that grow as $Z \to \infty$, we obtain expressions for the leading-order perturbing quantities in the upper deck

$$u_0^U = -\tfrac{\alpha_0 \sin\psi D}{\beta_0} e^{-\Gamma Z}, \qquad v_0^U = \tfrac{D}{x} e^{-\Gamma Z},$$
$$w_0^U = \tfrac{\mathrm{i}\sin\psi\Gamma D}{\beta_0} e^{-\Gamma Z}, \qquad p_0^U = De^{-\Gamma Z},$$
$$\rho_0^U = M_\infty^2 \sin^2\psi D e^{-\Gamma Z}, \qquad T_0^U = (\gamma-1)M_\infty^2 D e^{-\Gamma Z},$$

where D is some positive constant.

It is clear that we require $\Gamma^2 > 0$ to ensure the existence of physically relevant solutions and so have a condition that connects the local Mach number to the leading order wavenumbers,

$$\alpha_0^2 + \frac{\beta_0^2}{x^2\sin^2\psi}\left(1 - M_x^2\right) > 0.$$

For $0 \leqslant M_x < 1$, three-dimensional instability modes exist for all $\alpha_0,\beta_0 \in \mathbb{R}$. However, for $M_x > 1$, the condition imposes a restriction on the value of α_0 and β_0. As discussed by Hall (1986) and Seddougui

ψ	40°	50°	60°	70°	80°	90°
$(xM_\infty)_{\max}$	1.0075	1.2007	1.3574	1.4729	1.5436	1.5674

Table 1: The maximum value of xM_∞ for the existence of a stationary instability mode at each half-angle.

(1990), a further condition for the existence of instability modes is zero leading-order effective wall shear. That is, we require

$$\alpha_0 \left.\frac{\partial U}{\partial z}\right|_{z=0} + \frac{\beta_0}{x\sin\psi}\left.\frac{\partial V}{\partial z}\right|_{z=0} = 0, \tag{3..3}$$

where U and V are the steady flow quantities defined by the similarity solution Eq. (2..3). The similarity solution is such that

$$\left.\frac{\partial U}{\partial z}\right|_{z=0} = 0.51023 \quad \text{and} \quad \left.\frac{\partial V}{\partial z}\right|_{z=0} = -0.61592,$$

which, in Eq. (3..3), leads to

$$\frac{\alpha_0 x\sin\psi}{\beta_0} = 1.2071.$$

A necessary condition for the existence of the stationary mode is therefore found to be

$$0 \leqslant M_x < 1.5674.$$

Using Eq. (2..7) we note that, for fixed M_∞, this corresponds to a maximum radial distance from the axis of rotation, $r_{\max} = 1.5674/M_\infty$, which, in turn, determines a maximum distance along the cone, $x_{\max} = 1.5674/(M_\infty \sin\psi)$. These values are summarized in Table 1.

3.2. *Main-deck solutions*

The analysis of the main deck requires additional scalings to the wall-normal spatial variable and the perturbation quantities. In particular, we now let $z = \varepsilon^8\zeta$ such that $\zeta = \mathcal{O}(1)$ and use the expansions

$$\bar{u} = \varepsilon^{-1}u_0^M(\zeta) + u_1^M(\zeta) + \ldots,$$
$$\bar{w} = \varepsilon^3 w_0^M(\zeta) + \varepsilon^4 w_1^M(\zeta) + \ldots,$$

with the expansions for $\bar{v}, \bar{\rho}$ and $\bar{T}$ following $\bar{u}$, and $\bar{p}$ following $\bar{w}$. Here the superscript ^{M} is used to denote a quantity in the main deck.

We note that $p_0^U \to D$ as $Z \to 0$, and so, by Prantl matching across the upper and main deck, we find

$$\lim_{\zeta\to\infty} p_0^M(\zeta) = \lim_{Z\to 0} p_0^U(Z) = D.$$

Substituting the main-deck expansions into the governing perturbation equations results in leading-order equations at $\mathcal{O}\left(\varepsilon^{-5}\right)$. These can be combined to give ODEs in ζ that are solved to the obtain the leading-order perturbing quantities in the main deck,

$$u_0^M = \tfrac{\sin^2\psi\Gamma D x u'}{\beta_0^2}, \qquad v_0^M = \tfrac{\sin^2\psi\Gamma D x v'}{\beta_0^2},$$
$$w_0^M = -\tfrac{\mathrm{i}\sin^2\psi\Gamma D}{\beta_0^2}\left(\alpha_0 x u + \tfrac{\beta_0 v}{\sin\psi}\right), \qquad p_0^M = D,$$
$$\rho_0^M = \tfrac{\sin^2\psi\Gamma D}{\beta_0^2}\tfrac{\mathrm{d}\rho}{\mathrm{d}\zeta}, \qquad T_0^M = \tfrac{M_\infty^2(\gamma-1)\sin^2\psi\Gamma D}{\beta_0^2}\tfrac{\mathrm{d}T}{\mathrm{d}\zeta}.$$

Note that the constant D is that arising from the upper-deck analysis.

The wall-normal velocity w_0^M satisfies the usual no-slip condition at $\zeta = 0$, whereas u_0^M and v_0^M do not. Therefore we impose the following constraint arising from Eq. (3..3)

$$\alpha_0 \bar{u}_0 + \frac{\beta_0 \bar{v}_0}{x \sin\psi} = 0 \Rightarrow \frac{\alpha_0 x \sin\psi}{\beta_0} = -\frac{\bar{v}_0}{\bar{u}_0}, \tag{3..4}$$

then $\alpha_0 u_0^M + \beta_0 v_0^M / x \sin\psi \to 0$ as $\eta \to 0$. It is this imposition that forces us to consider only stationary disturbances.

3.3. *Lower-deck solutions*

3.3..1 Leading order

We now use $z = \varepsilon^9 \xi$, such that $\xi = \mathscr{O}(1)$ in the lower deck. Here it is necessary to introduce expansions for both the steady and perturbing quantities.

For small ζ we expand the basic-flow components U, V, W, ρ and T and these are given in terms of ξ as

$$\begin{aligned} U &= \varepsilon u_0 \xi + \varepsilon^2 u_1 \xi^2 + \varepsilon^3 u_2 + \ldots, \\ \rho &= \rho_w + \varepsilon \rho_0 \xi + \varepsilon^2 \rho_1 \xi^2 + \ldots, \end{aligned}$$

with the expansion for V and W following that of U, and T following ρ. Each basic-flow term is now given by

$$u_{j-1} = \frac{1}{j!} \left. \frac{\partial^j u}{\partial z^j} \right|_{\zeta=0},$$

with equivalent expressions for v_{j-1}, ρ_{j-1} and T_{j-1}. Note that the subscript $_w$ denotes the value of the quantity at the cone surface.

The lower-deck perturbation quantities are expanded as

$$\begin{aligned} \bar{u} &= \frac{u_{-1}^L(\xi)}{\varepsilon} + u_0^L(\xi) + \varepsilon u_1^L(\xi) + \ldots, \\ \bar{w} &= \varepsilon^3 w_0^L(\xi) + \varepsilon^4 w_1^L(\xi) + \ldots, \end{aligned}$$

where the expansions for $\bar{v}, \bar{\rho}$ and $\bar{T}$ follow $\bar{u}$, and $\bar{p}$ follows $\bar{w}$. Here the superscript ^{L} is used to denote a quantity in the lower deck.

Matching with the leading-order terms from the main-deck solutions, and substituting the basic-flow expansions, we obtain the lower-deck perturbation terms for substitution into the governing perturbation equations. Subsequently equating terms of $\mathscr{O}(\varepsilon^{-3})$ in the streamwise perturbation equation leads to a governing ODE in ξ for $u_{-1}^L(\xi)$ given by

$$\frac{\mathrm{d}^2 u_{-1}^L}{\mathrm{d}\xi^2} - \mathrm{i}\rho \left(\alpha_0 x u_1 + \frac{\beta_0 v_1}{\sin\psi} \right) \xi^2 u_{-1}^L = 0, \tag{3..5}$$

which is subject to the conditions of no-slip at the cone wall and zero wall-normal perturbation at $\mathscr{O}(\varepsilon^{-1})$,

$$\begin{aligned} u_{-1}^L &= -\frac{\sin^2\psi x \Gamma D u_0}{\beta_0^2} \qquad \text{at} \qquad \xi = 0, \\ u_{-1}^L &\to 0 \qquad \text{as} \qquad \xi \to \infty. \end{aligned}$$

Progress in the solution of Eq. (3..5) can be made using the substitution $\nu = \sqrt{2}\Delta^{\frac{1}{4}}\xi$, where

$$\Delta = \frac{\mathrm{i}}{T_w}\left(\alpha_0 x u_1 + \frac{\beta_0 v_1}{\sin\psi}\right).$$

This leads to a parabolic cylinder ODE in ν for u^L_{-1},

$$\frac{\mathrm{d}u^L_{-1}}{\mathrm{d}\nu^2} - \frac{\rho^2}{4}u^L_{-1} = 0,$$

subject to

$$u^L_{-1} = -\frac{\sin^2\psi x \Gamma D u_0}{\beta_0^2} \qquad \text{at} \qquad \nu = 0,$$
$$u^L_{-1} \to 0 \qquad \text{as} \qquad \nu \to \infty,$$

which is solved to yield

$$u^L_{-1}(\xi) = -\frac{\sin^2\psi x \Gamma D u_0}{\beta_0^2}\frac{U_c\left(0, \sqrt{2}\Delta^{\frac{1}{4}}\xi\right)}{U(0,0)}.$$

Here U_c is the parabolic cylinder function as defined by Abramowitz & Stegun (1964).

A similar analysis of the other perturbation equations at leading order can be performed to yield

$$v^L_{-1}(\xi) = \frac{\alpha_0 \sin^3\psi x^2 \Gamma D u_0}{\beta_0^3}\frac{U_c\left(0, \sqrt{2}\Delta^{\frac{1}{4}}\xi\right)}{U_c(0,0)},$$
$$T^L_{-1}(\xi) = -\frac{\sin^2\psi \Gamma D T_0}{\beta_0^2}\frac{U_c\left(0, \sqrt{2}\sigma^{\frac{1}{4}}\Delta^{\frac{1}{4}}\xi\right)}{U_c(0,0)},$$
$$\rho^L_{-1}(\xi) = -\frac{\sin^2\psi \Gamma D \rho_0}{\beta_0^2}\frac{U_c\left(0, \sqrt{2}\sigma^{\frac{1}{4}}\Delta^{\frac{1}{4}}\xi\right)}{U_c(0,0)}.$$

3.3..2 Next order

We now proceed to determine leading-order estimates of the effective wavenumber and waveangle of the stationary disturbances. In order to determine these quantities, we will see that it is necessary to proceed with the analysis of the lower deck at the next order. In what follows, it will be useful to define the scaled leading-order wavenumber as

$$\gamma_0 = \left(\alpha_0^2 + \frac{\beta_0^2}{x^2\sin^2\psi}\right)^2,$$

and the waveangle by ϕ, such that

$$\tan\left(\frac{\pi}{2} - \phi\right) = \frac{\alpha x}{\beta}.$$

Using the expansions detailed in §3.3..1, the steamwise and azimuthal perturbation equations in the lower deck at $\mathscr{O}(\varepsilon^{-3})$ are combined in such a way to give an ODE in ξ for w_0^L that involves γ_0. Full details are given by Towers (2013) and, although not shown here, the resulting ODE is solved to give

$$w_0^L = -\mathrm{i}\left(\alpha_1 x u_0 + \frac{\beta_1 v_0}{\sin\psi}\right)\frac{\Gamma\sin^2\psi}{\beta_0^2} + k_1\xi^2 + \Delta^{-\frac{3}{4}}\left\{\gamma_0^2 DF_1(s) + \frac{2\mathrm{i}\gamma_0^2\Gamma x\sin^3\psi Du_0}{\beta_0^3 T_w U(0,0)}F_2(s) - \frac{3\mathrm{i}\alpha_0\Gamma x\sin^2\psi D\rho_0}{\beta_0^2 U(0,0)}F_3(s) + \frac{\mathrm{i}(1-\sigma)\alpha_0\Gamma x\sin^2\psi D\rho}{2\beta_0^2 U(0,0)}F_4(s)\right\},$$

where k_1 is a constant and $s = \Delta^{\frac{1}{4}}\xi$. Furthermore, $F_i(s)$ (for $i = 1,\ldots,4$) satisfy the following ODEs in ξ

$$F_1''' - s^2F_1' + 2sF_1 = 1, \tag{3..6}$$

$$F_2''' - s^2F_2' + 2sF_2 = U_c\left(0,\sqrt{2}\sigma^{\frac{1}{4}}s\right), \tag{3..7}$$

$$F_3''' - s^2F_3' + 2sF_3 = \frac{\mathrm{d}}{\mathrm{d}s}\left(sU_c\left(0,\sqrt{2}\sigma^{\frac{1}{4}}s\right)\right), \tag{3..8}$$

$$F_4''' - s^2F_4' + 2sF_4 = s^4U_c\left(0,\sqrt{2}\sigma^{\frac{1}{4}}s\right), \tag{3..9}$$

subject to the boundary conditions $F_i(0) = F_i(\infty) = 0$.

Some further manipulation involving use of the continuity equation at $\mathscr{O}(\varepsilon^{-3})$, leads to

$$\gamma_0^2F_1'(0) = \frac{\Gamma\sin^2\psi(\alpha_0 x)^{\frac{1}{2}}}{2\beta_0^2T_w}\left(\alpha_1u_0 + \frac{\beta_1v_0}{x\sin\psi}\right), \tag{3..10}$$

$$\frac{2\gamma_0^2\Gamma x\sin^3\psi u_0}{\beta_0^3T_wU_c(0,0)}F_2'(0) - \frac{3\alpha_0\Gamma x\sin^2\psi\rho_0}{\beta_0^2U_c(0,0)}F_3'(0) + \frac{(1-\sigma)\alpha_0\Gamma x\sin^2\psi\rho_0}{2\beta_0^2U_c(0,0)}F_4'(0) = \frac{\Gamma\sin^2\psi(\alpha_0x)^{\frac{1}{2}}}{2\beta_0^2T_w}\left(\alpha_1u_0 + \frac{\beta_1v_0}{x\sin\psi}\right), \tag{3..11}$$

which can be combined to determine an eigenrelation for γ_0. Specifically we arrive at

$$\gamma_0^2F_1'(0) - \frac{2\gamma_0^2\Gamma x\sin^3\psi u_0}{\beta_0^3T_2U_c(0,0)}F_2'(0) + \frac{3\alpha_0\Gamma x\sin^2\psi\rho_0}{\beta_0^2U_c(0,0)}F_3'(0) - \frac{(1-\sigma)\alpha_0\Gamma x\sin^2\psi\rho_0}{2\beta_0^2U_c(0,0)}F_4'(0) = 0. \tag{3..12}$$

The values of $F_i'(0)$ are obtained from the solutions of Eqs. (3..6)–(3..9). These are solved by following the method developed by Hall (1986) and fully outlined more recently by Hussain (2008). In particular, we transform the equations such that they can be solved using parabolic cylinder equations and determine that

$$F_1'(0) = 0.5984, \qquad F_2'(0) = 0.2779,$$
$$F_3'(0) = 0.0192, \qquad F_4'(0) = 1.6972.$$

The values for $F_3'(0)$ and $F_4'(0)$ depend on σ and we have chosen $\sigma = 0.7$ (consistent with air). Note that the value found for $F_1'(0)$ is in agreement with Hussain (2008) but differs slightly from the value 0.5991 found by Hall (1986) and Seddougui (1990). As discussed by Hussain, this is likely due to the choice of integration method employed.

We proceed by imposing the condition of zero leading-order effective wall shear, Eq. (3..4), and rewrite Eq. (3..12) to obtain

$$\gamma_0 = \frac{1}{\sqrt{F_1'(0)}}\left(1+\frac{v_0^2}{u_0^2}-M_x^2\right)^{\frac{1}{4}}\left(\frac{2u_0F_2'(0)}{T_w^2 x U_c(0,0)}\left(1+\frac{v_0^2}{u_0^2}\right)+\frac{3v_0\rho_0F_3'(0)}{u_0 x U_c(0,0)}-\frac{(1-\sigma)v_0\rho_0F_4'(0)}{2u_0 x U_c(0,0)}\right)^{\frac{1}{2}}.$$

The equation of state gives $\rho_0 = -\frac{T_0}{T_w^2}$ and we proceed to use the temperature relation Eq. (2..8) to determine that

$$T_0 = -\frac{\gamma-1}{2}M_x^2 f'(0) + (T_w-1)q'(0),$$

where $f'(0) = -0.4562$ and $q'(0) = -0.3241$ are obtained numerically in the particular case that $\sigma = 0.7$. Collectively these enable us to determine that

$$\gamma_0 = \frac{1.293x^{-\frac{1}{2}}}{T_w}\left(2.457-M_x^2\right)^{\frac{1}{4}}\left(0.573+0.310T_0\right)^{\frac{1}{2}}, \tag{3..13}$$

where

$$T_0 = 0.091M_x^2 - 0.324(T_w-1).$$

Equation (3..13) gives our leading-order estimate of the wavenumber in terms of the lower-deck scalings and ε.

Proceeding along similar lines, it is possible to work with Eq. (3..10) to determine an expression towards the waveangle estimate given by

$$\left(\frac{\alpha_1}{\beta_0}-\frac{\alpha_0\beta_1}{\beta_0^2}\right) = \frac{1}{\sin\psi}\frac{2\gamma^{\frac{3}{2}}T_w^2F_1'(0)}{|u_0v_0|^{\frac{1}{2}}x^{\frac{1}{2}}}\left(1+\frac{v_0^2}{u_0^2}-M_x^2\right)^{-\frac{1}{2}}\left(1+\frac{v_0^2}{u_0^2}\right),$$

which, after substituting all known values, leads to

$$\left(\frac{\alpha_1}{\beta_0}-\frac{\alpha_0\beta_1}{\beta_0^2}\right) = \frac{1}{\sin\psi}\frac{2.669\gamma_0^{\frac{3}{2}}T_w^2}{x^{\frac{1}{2}}\left(2.457-M_x^2\right)^{\frac{1}{2}}}. \tag{3..14}$$

As discussed by Hussain (2008), it is not possible to find α_1 and β_1 independently from this analysis. Instead we concentrate on the combination of α_1 and β_1 found in Eq. (3..14) in terms of ϕ. This approach leads to

$$\begin{aligned}\tan\left(\frac{\pi}{2}-\phi\right) = \frac{\alpha x}{\beta} &= \frac{\left(\alpha_0+\varepsilon^2\alpha_1+\ldots\right)x}{\left(\beta_0+\varepsilon^2\beta_1+\ldots\right)},\\ &= \frac{\alpha_0 x}{\beta_0}+\varepsilon^2\left(\frac{\alpha_1}{\beta_0}-\frac{\alpha_0\beta_1}{\beta_0^2}\right)x,\\ &= \frac{1.207}{\sin\psi}+\varepsilon^2\left(\frac{\alpha_1}{\beta_0}-\frac{\alpha_0\beta_1}{\beta_0^2}\right)x.\end{aligned}$$

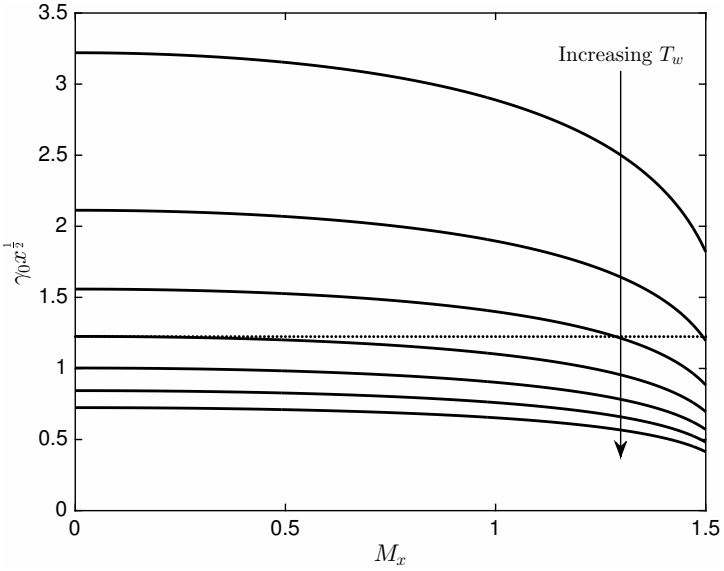

FIG. 1: The effective wavenumber $\gamma_0 x^{\frac{1}{2}}$ for fixed $T_w = 0.4, 0.6, \ldots, 1.6$. The dotted line gives the incompressible case.

Using Eq. (3..14) to obtain the waveangle correction, we determine that

$$\tan\left(\frac{\pi}{2} - \phi\right) = \frac{1.207}{\sin\psi} + \frac{\varepsilon^2 x}{\sin\psi} \frac{2.669\gamma_0^{\frac{3}{2}} T_w^2}{x^{\frac{1}{2}} (2.457 - M_x^2)^{\frac{1}{2}}}. \tag{3..15}$$

Equation (3..15) gives our leading-order estimate for the waveangle in terms of ε.

Figure 1 shows $\gamma_0 x^{\frac{1}{2}}$ as a function of local Mach number M_x for various wall temperatures T_w. This quantity is interpreted as the scaled leading-order effective wavenumber of the disturbances and is obtained directly from Eq. (3..13). We see that the effective wavenumber of the disturbances decreases with increased local Mach number, M_x. Note that the dependence of $\gamma_0 x^{\frac{1}{2}}$ on the half-angle appears only in the definition of the M_x (see Eq. 2..7), and the figure is therefore directly comparable with the results of Seddougui (1990) for the rotating disk with isothermal wall. We find qualitative agreement with Fig. 1 of Seddougui's paper and the slight quantitative differences arise from the use of $\sigma = 0.7$ here compared to her 0.72. In the particular case that $T_w = 1$ and $M_x << 1$, we find excellent agreement with the incompressible case of $\gamma_0 x^{\frac{1}{2}} = 1.224$ due to Hall (1986). For $T_w > 1$, the wavenumber is lower than that for the incompressible case, which means that disturbances in the compressible flow have a larger wavelength than in the incompressible flow. The opposite is true for $T_w < 1$, suggesting that wall cooling could be viewed as a stabilising feature. This behaviour is in agreement with the conclusions of Seddougui (1990) for the rotating disk.

Figure 2 shows the waveangle correction at the next order as a function of M_x for various T_x; this

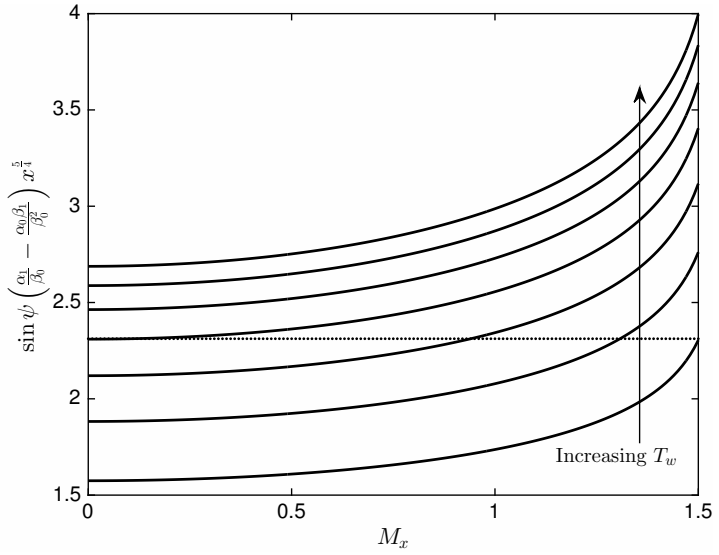

FIG. 2: The waveangle correction for fixed $T_w = 0.4, 0.6, \ldots, 1.6$. The dotted line gives the incompressible case.

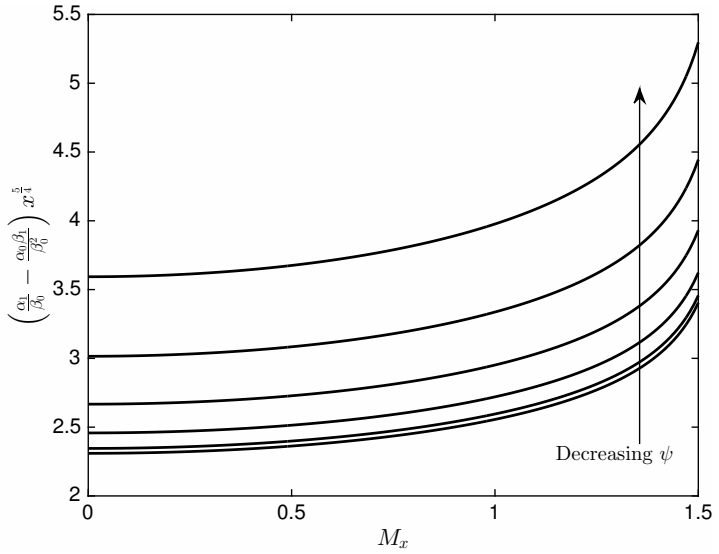

FIG. 3: The waveangle correction for $T_w = 1$ for $\psi = 90^\circ, 80^\circ, \ldots, 40^\circ$.

follows directly from Eq. (3..14). Note that this quantity is not independent of the half-angle, however the results are presented with $\sin\psi$ scaled out and so correspond to the case of the rotating disk. These results are in qualitative agreement with Fig. 2 of Seddogui's paper on the rotating disk and any slight quantitative differences are attributed to the value of σ. We again note that for $T_w = 1$ and $M_x << 1$ our results are in excellent agreement with Hall's incompressible result that the correction term has value 2.312. The results suggest that, at fixed ψ, the waveangle decreases as the local Mach number increases for the values of T_w considered here. The effect of ψ on this correction is presented in Figure 3 for $T_w = 1$. We see that, at this wall temperature and all others, the wave angle decreases as the half-angle decreases. Our predictions are discussed further in §§4. & 5..

4. Waveangle and wavenumber predictions

We now seek to express our estimates of wavenumber and waveangle in the lower deck, Eqs. (3..13) and (3..15), in terms of physical boundary-layer parameters. In particular, we note that the expansion of the local wavenumber used in §3.3..2 is scaled on the viscous-mode wavelength and so, at leading order, is actually given by $\varepsilon^4\gamma_0$. Using Eq. (3..13), we therefore have a leading-order estimate of the wavenumber given by

$$\varepsilon^4\gamma_0 = \frac{\varepsilon^4 1.293 x^{-\frac{1}{2}}}{T_w}\left(2.457 - M_x^2\right)^{\frac{1}{4}}\left(0.573 + 0.310T_0\right)^{\frac{1}{2}}. \tag{4..1}$$

Following Garrett *et al.* (2009), we define a Reynolds number based on the boundary-layer thickness δ^*, given by

$$R_{\delta^*} = Re^{\frac{1}{2}} x(\sin\psi)^{\frac{1}{2}}, \tag{4..2}$$

and can express this local wavenumber estimate as

$$\gamma_{\delta^*} = \frac{1.293 R_{\delta^*}^{-\frac{1}{2}}(\sin\psi)^{\frac{1}{4}}}{T_w}\left(2.457 - M_x^2\right)^{\frac{1}{4}}\left(0.573 + 0.310T_0\right)^{\frac{1}{2}}. \tag{4..3}$$

Furthermore, using Eq. (3..15) the local waveangle estimate can be written as

$$\tan\left(\frac{\pi}{2} - \phi\right) = \frac{1.207}{\sin\psi} + \frac{3.924 R_{\delta^*}^{\frac{1}{4}} T_w^{\frac{1}{2}}\left(0.573 + 0.310_0\right)^{\frac{3}{4}}}{(\sin\psi)^{\frac{7}{8}}\left(2.457 - M_x^2\right)^{\frac{1}{8}}}. \tag{4..4}$$

Equations (4..1) and (4..4) are our estimates of the wavenumber and waveangle, expressed in terms of boundary-layer parameters. The appearance of the wall temperature, half-angle and local Mach number allow us to consider the effects of both compressibility and cone geometry on the stability characteristics on the flow.

Figures 4–6 show the asymptotic wavenumber and waveangle predictions for neutrally stable disturbances as a function of local Reynolds number, R_{δ^*}. Recall from Eq. (2..1) that, for a particular cone, an increase in the (basic) Reynolds number, Re, corresponds to an increased rotation rate Ω^*. Using Eq. (4..2), we see that an increase in the local Reynolds number therefore corresponds to either an increase in rotation rate or an increase in streamwise location, x, at which the local analysis is performed.

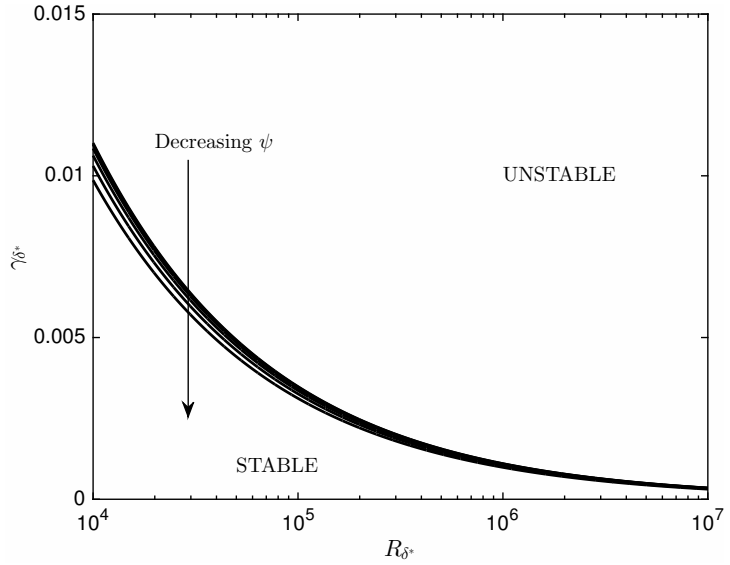

(a) Wavenumber predictions

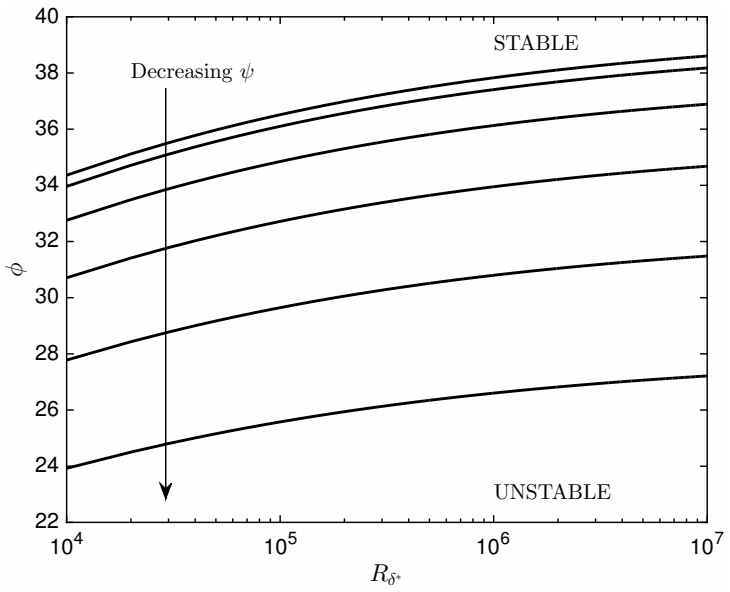

(b) Waveangle predictions

FIG. 4: Asymptotic predictions for viscous Type II modes for fixed $T_w = M_x = 1$ and $\psi = 90^\circ, 80^\circ, \ldots, 40^\circ$.

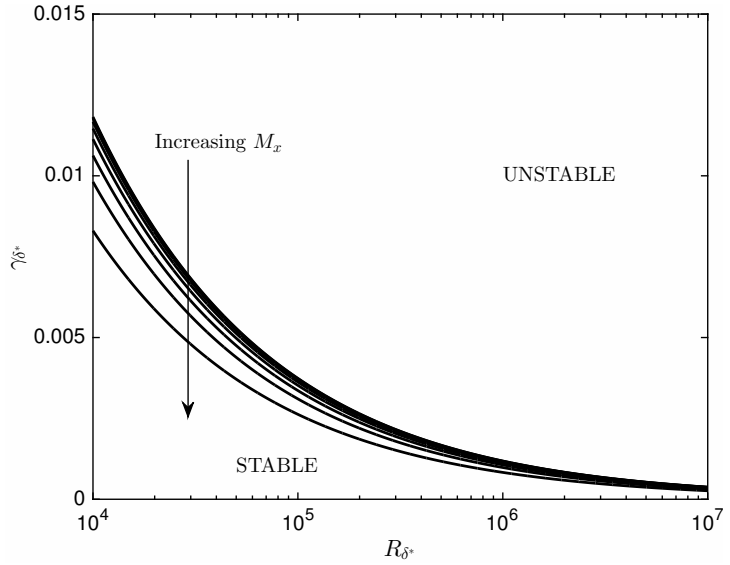

(a) Wavenumber predictions

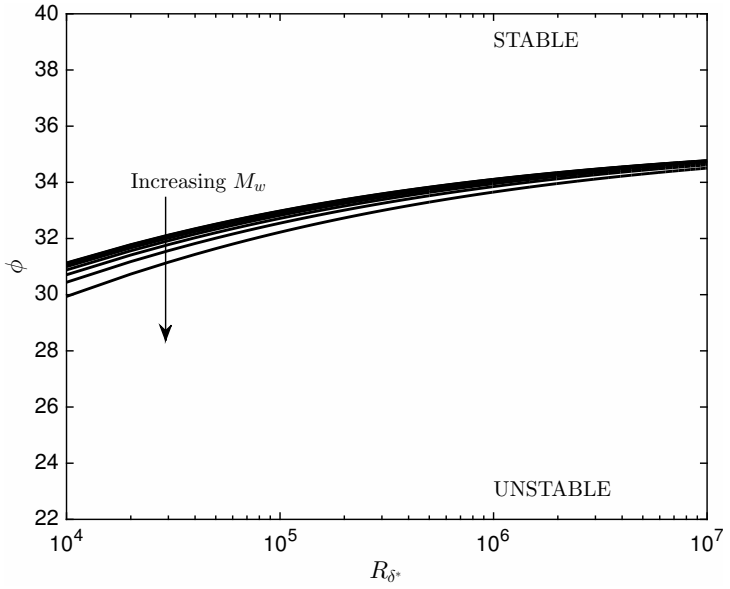

(b) Waveangle predictions

FIG. 5: Asymptotic predictions for viscous Type II modes for fixed $\psi = 60^\circ$, $T_w = 1$ and $M_x = 0, 0.2, \ldots, 1.4$.

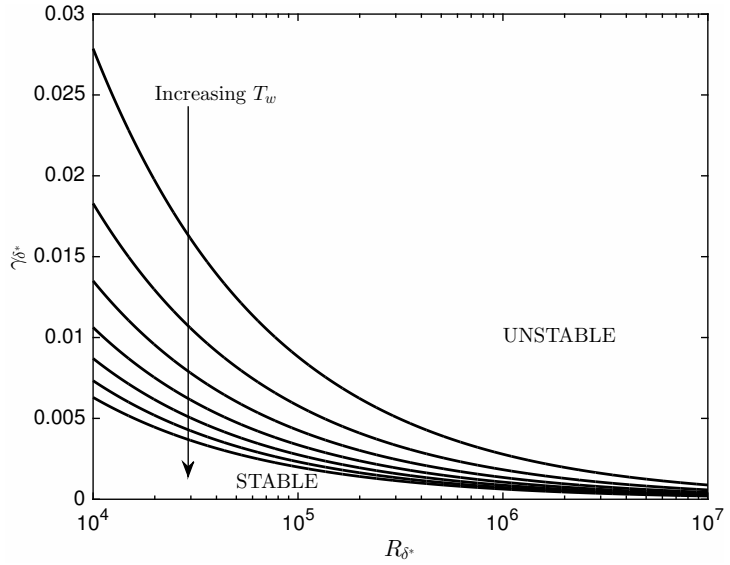

(a) Wavenumber predictions

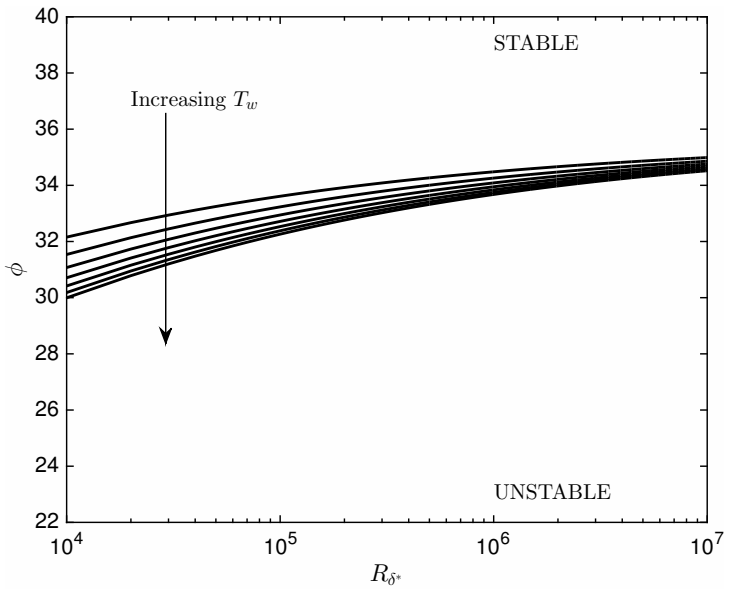

(b) Waveangle predictions

FIG. 6: Asymptotic wavenumber and waveangle predictions for viscous Type II modes for fixed $\psi = 60^\circ$, $M_x = 1$ and $T_w = 0.4, 0.6, \ldots, 1.6$.

However, given that the local Mach number (Eq. 2..7) is also dependent on x, we shall assume that all analyses have been conducted at the location of fixed radial position, $r = x\sin\psi$, and so an increase in R_{δ^*} corresponds to an increase in the rotation rate.

In Figure 4, the effect of half-angle ψ is demonstrated at fixed wall temperature T_w and local Mach number M_x. In Figure 5 we see the effect of M_x for fixed T_w and ψ, and in Figure 6 we see the effect of T_w for fixed M_x and ψ. Recall from the analysis of the upper deck in §3.1. that the maximum value of M_x is 1.5674 and so the range of M_x used in Figure 5 is appropriate. The parameter regimes for stable and unstable flows are indicated in each figure and note that the regions are reversed when moving between the γ_{δ^*} and ϕ plots. That is, the curves represent the lower branch of the neutral curve in the R_{δ^*}–γ_{δ^*} plane, and the upper branch in the R_{δ^*}–ϕ plane. This is consistent with the interpretation of the viscous Type II mode arising in the neutral curves presented by Garrett *et al.* (2009), for example, for the incompressible case.

It is difficult make conclusive statements about the stabilising nature (or otherwise) of particular flow parameters without access to full neutral curves where the behaviour of the critical Reynolds numbers and inviscid branch can be seen. We are however able to make some conjectures on the basis that a perceived narrowing of the unstable parameter region in the R_{δ^*}–γ_{δ^*} plane corresponds to a stabilising effect. This of course assumes that the (upper) inviscid branch does not move in opposition to this narrowing of the unstable wavenumber region. A leading-order analysis of that mode has been performed by Towers & Garrett (2012) and suggests that this assumption is valid. A narrowing of the unstable region expressed in terms of the waveangle is taken to be of less importance as that merely indicates the way an unstable mode might wrap around the cone surface.

Figure 4 suggests that, although the disturbance waveangle is particularly sensitive to half-angle, decreasing ψ has only a marginal effect on the stability of the flow. This is consistent with the incompressible results of Garrett *et al.* (2009). Figure 5 demonstrates that increasing the local Mach number is marginally destabilising and has little effect on the disturbance waveangle. In contrast, Figure 6 suggests that the stability of the compressible flow is particularly sensitive to the wall temperature of the cone. Wall-cooling appears to be an effective stabilising mechanism, consistent with the conclusion of the rotating-disk study by Seddougui (1990). We note that the disturbance waveangle demonstrates only marginal sensitivity to wall temperature.

5. Conclusion

We have presented a high-Reynolds-number asymptotic analysis of the viscous instability mode (Type II) within the boundary layer over broad, rotating cones. The steady flows used were those previously obtained by Towers & Garrett (2014) and are known to be consistent with the compressible rotating-disk flows obtained by Seddougui and Turkyilmazoglu *et al.* (2000).

The analysis presented here was formulated using scalings consistent with the equivalent but incompressible analysis of Garrett *et al.* (2009). These scalings remove the explicit appearance of the cone half-angle and a direct comparison can be made with the previous asymptotic analysis of the compressible boundary-layer flow over the rotating disk due to Seddougui (1990). Our conclusions are entirely comparable with those of Seddougui and any slight numerical differences between the two analyses are attributed to different values used for σ and γ.

A key result of our analysis is that stationary, three-dimensional stationary modes do not exist beyond a particular local Mach number of $M_x = 1.5674$. This numerical prediction is identical to the results of Seddougui and we are further able to determine the effects of reducing the cone half-angle. Furthermore, we predict that the stability characteristics of the boundary-layer flow at all half-angles

are particularly sensitive to wall temperature. It is suggested that wall-cooling is an effective stabilising mechanism for the Type II mode.

Our analysis has assumed that the cone is rotating in air, and hence we have set the flow parameters to $\sigma = 0.7$ and $\gamma = 1.4$ throughout the analysis. Most gases have values $\sigma \sim 0.16$–0.8 and $\gamma \sim 1$–1.7, and we expect that changes in these parameters would not cause significant changes in our results. That is, similar qualitative conclusions are expected for all reasonable combinations of σ and γ.

A leading-order analysis of the inviscid (Type I) mode has been performed by Towers & Garrett (2012). The indications of that preliminary analysis appear to suggest that a reduction in half-angle acts to destabilise the inviscid mode. This is consistent with the results of this analysis of the viscous mode. A reduced half-angle is therefore seen to be marginally stabilising for both the incompressible (Garrett *et al.* 2009) and compressible boundary-layer flows.

Funding

This work was supported by the Engineering and Physical Sciences Research Council (grant EP/G061637/1), and the Royal Academy of Engineering (LSRF1415/11/29).

A Linear perturbation equations

The linearized perturbation equations for the compressible rotating cone system are presented for completeness. Perturbation quantities are indicated with a tilde.

$$\begin{aligned}&\Big(xu\frac{\partial}{\partial x}+\frac{xv}{h}\frac{\partial}{\partial\theta}+R^{-\frac{1}{2}}w\frac{\partial}{\partial z}+u+R^{-\frac{1}{2}}\frac{\partial w}{\partial z}+\frac{xu\sin\psi}{h}+\frac{R^{-\frac{1}{2}}w\cos\psi}{h}\Big)\tilde{\rho}\\&+\Big(\frac{\partial\tilde{u}}{\partial x}+\frac{1}{h}\frac{\partial\tilde{v}}{\partial\theta}\Big)\rho+\Big(\frac{\partial\rho}{\partial x}+\frac{\rho\sin\psi}{h}\Big)\tilde{u}+\Big(\frac{\partial\rho}{\partial z}+\rho\frac{\partial}{\partial z}+\frac{\rho\cos\psi}{h}\Big)\tilde{w}=0,\end{aligned}\tag{A.1}$$

$$\begin{aligned}&\rho\Big\{\Big(xu\frac{\partial}{\partial x}+\frac{xv}{h}\frac{\partial}{\partial\theta}+R^{-\frac{1}{2}}w\frac{\partial}{\partial z}+u\Big)\tilde{u}-2\Big(\frac{v\sin\psi}{h}+1\Big)\tilde{v}+x\tilde{w}\frac{\partial u}{\partial z}\Big\}\\&\quad+\tilde{\rho}\Big(xu^2+R^{-\frac{1}{2}}xw\frac{\partial u}{\partial z}-\frac{x^2v^2\sin\psi}{h}-2xv-\frac{h}{\sin\psi}\Big)=-\frac{\partial\tilde{p}}{\partial x}\\&\quad+\frac{1}{R}\Big\{2\frac{\partial}{\partial x}\Big(T\frac{\partial\tilde{u}}{\partial x}+\tilde{T}u\Big)+\frac{1}{h}\frac{\partial}{\partial\theta}\Big(T\Big(\frac{\partial\tilde{v}}{\partial x}+\frac{1}{h}\frac{\partial\tilde{u}}{\partial\theta}-\frac{\tilde{v}\sin\psi}{h}\Big)\\&\qquad+\tilde{T}\Big(v-\frac{xv\sin\psi}{h}\Big)\Big)+\frac{\partial}{\partial z}\Big(T\Big(\frac{\partial\tilde{w}}{\partial x}+\frac{\partial\tilde{u}}{\partial z}\Big)+\tilde{T}x\frac{\partial u}{\partial z}\Big)\Big\},\end{aligned}\tag{A.2}$$

$$\begin{aligned}
&\rho\Big\{\Big(xu\frac{\partial}{\partial x}+\frac{xv}{h}\frac{\partial}{\partial\theta}+R^{-\frac{1}{2}}w\frac{\partial}{\partial z}+\frac{xu\sin\psi}{h}+\frac{R^{-\frac{1}{2}}w\cos\psi}{h}\Big)\tilde{v} \\
&\qquad+\Big(\tilde{w}x\frac{\partial}{\partial z}+\frac{\tilde{u}x\sin\psi}{h}+\frac{\tilde{w}x\cos\psi}{h}+\tilde{u}\Big)v+2(\tilde{u}+\tilde{w}\cot\psi)\Big\} \\
&+\tilde{\rho}\Big\{\Big(R^{-\frac{1}{2}}xw\frac{\partial}{\partial z}+xu+\frac{x^2u\sin\psi}{h}+\frac{R^{-\frac{1}{2}}w\cos\psi}{h}\Big)v+2(xu+R^{-\frac{1}{2}}w\cot\psi)\Big\} \\
&\qquad=\frac{-1}{h}\frac{\partial\tilde{p}}{\partial\theta}+\frac{1}{R}\Big\{\frac{\partial}{\partial x}\Big(T\Big(\frac{\partial\tilde{v}}{\partial x}+\frac{1}{h}\frac{\partial\tilde{u}}{\partial\theta}-\frac{\tilde{v}\sin\psi}{h}\Big)+\tilde{T}\Big(v-\frac{xv\sin\psi}{h}\Big)\Big) \\
&\qquad+\frac{2}{h^2}\frac{\partial}{\partial\theta}\Big(T\Big(\frac{\partial\tilde{v}}{\partial\theta}+\tilde{u}\sin\psi+\tilde{w}\cos\psi\Big)+\tilde{T}\Big(xu\sin\psi+R^{-\frac{1}{2}}w\cos\psi\Big)\Big) \\
&\qquad+\frac{\partial}{\partial z}\Big(T\Big(\frac{\partial\tilde{v}}{\partial z}+\frac{1}{h}\frac{\partial\tilde{w}}{\partial\theta}-\frac{\tilde{v}\cos\psi}{h}\Big)+\tilde{T}\Big(x\frac{\partial v}{\partial z}-\frac{xv\cos\psi}{h}\Big)\Big)\Big\},
\end{aligned}\tag{A.3}$$

$$\begin{aligned}
&\rho\Big\{\Big(xu\frac{\partial}{\partial x}+\frac{xv}{h}\frac{\partial}{\partial\theta}+R^{-\frac{1}{2}}w\frac{\partial}{\partial z}+R^{-\frac{1}{2}}\frac{\partial w}{\partial z}\Big)\tilde{w}-2\Big(\frac{xv\cos\psi}{h}+\cot\psi\Big)\tilde{v}\Big\} \\
&\qquad+\tilde{\rho}\Big(R^{-1}w\frac{\partial w}{\partial z}-\frac{x^2v^2\cos\psi}{h}-2xv\cot\psi-\frac{h\cot\psi}{\sin\psi}\Big)=-\frac{\partial\tilde{p}}{\partial z} \\
&+\frac{1}{R}\Big\{\frac{\partial}{\partial x}\Big(T\Big(\frac{\partial\tilde{w}}{\partial x}+\frac{\partial\tilde{u}}{\partial z}\Big)+\tilde{T}x\frac{\partial u}{\partial z}\Big)+\frac{1}{h}\frac{\partial}{\partial\theta}\Big(T\Big(\frac{\partial\tilde{v}}{\partial z}+\frac{1}{h}\frac{\partial\tilde{w}}{\partial\theta}-\frac{\tilde{v}\cos\psi}{h}\Big) \\
&\qquad+\tilde{T}\Big(x\frac{\partial v}{\partial z}-\frac{xv\cos\psi}{h}\Big)\Big)+2\frac{\partial}{\partial z}\Big(T\frac{\partial\tilde{w}}{\partial z}+R^{-\frac{1}{2}}\tilde{T}\frac{\partial w}{\partial z}\Big)\Big\},
\end{aligned}\tag{A.4}$$

$$\gamma M_\infty^2\tilde{p}=\tilde{\rho}T+\rho\tilde{T},\tag{A.5}$$

$$\frac{\rho}{M_\infty^2(\gamma-1)}\Big(u x\frac{\partial\tilde{T}}{\partial x}+\tilde{u}\frac{\partial T}{\partial x}+\frac{xv}{h}\frac{\partial\tilde{T}}{\partial\theta}+R^{-\frac{1}{2}}w\frac{\partial\tilde{T}}{\partial z}+\tilde{w}\frac{\partial T}{\partial z}\Big) \tag{A.6}$$

$$+\frac{\tilde{\rho}}{M_\infty^2(\gamma-1)}\Big(xu\frac{\partial T}{\partial x}+R^{-\frac{1}{2}}w\frac{\partial T}{\partial z}\Big)=xu\frac{\partial\tilde{p}}{\partial x}+\tilde{u}\frac{\partial p}{\partial x}+\frac{xv}{h}\frac{\partial\tilde{p}}{\partial\theta}+R^{-\frac{1}{2}}w\frac{\partial\tilde{p}}{\partial z}$$

$$+\tilde{w}\frac{\partial p}{\partial z}+\frac{1}{h\sigma RM_\infty^2(\gamma-1)}\Big\{\frac{\partial}{\partial x}\Big(h\frac{\partial\tilde{T}}{\partial x}\Big)+\frac{\partial^2\tilde{T}}{\partial\theta^2}+\frac{\partial}{\partial z}\Big(h\frac{\partial\tilde{T}}{\partial z}\Big)\Big\}$$

$$+\frac{\mu}{R}\Big\{2u\frac{\partial\tilde{u}}{\partial x}+\frac{2}{h^2}\Big((xu\sin\psi+R^{-\frac{1}{2}}w\cos\psi)\frac{\partial\tilde{v}}{\partial\theta}+(xu\sin\psi$$

$$+R^{-\frac{1}{2}}w\cos\psi)\tilde{u}\sin\psi+(xu\sin\psi+R^{-\frac{1}{2}}w\cos\psi)\tilde{w}\cos\psi)+2w\frac{\partial\tilde{w}}{\partial z}$$

$$+2R^{-\frac{1}{2}}\frac{\partial w}{\partial z}\frac{\partial\tilde{w}}{\partial z}+\Big(v-\frac{xv\sin\psi}{h}\Big)\frac{\partial\tilde{v}}{\partial x}+\Big(\frac{v}{h}-\frac{xv\sin\psi}{h^2}\Big)\frac{\partial\tilde{u}}{\partial\theta}$$

$$+\Big(\frac{xv\sin^2\psi}{h}-\frac{v\sin\psi}{h}\Big)\tilde{v}+x\frac{\partial u}{\partial z}\frac{\partial\tilde{u}}{\partial z}+x\frac{\partial u}{\partial z}\frac{\partial\tilde{w}}{\partial x}+\Big(v+x\frac{\partial v}{\partial z}-\frac{xv\cos\psi}{h}\Big)\frac{\partial\tilde{v}}{\partial z}$$

$$+\Big(\frac{v}{h}+\frac{x}{h}\frac{\partial v}{\partial z}-\frac{xv\cos\psi}{h^2}\Big)\frac{\partial\tilde{w}}{\partial\theta}+\Big(\frac{xv\cos^2\psi}{h}-\frac{x\cos\psi}{h}\frac{\partial v}{\partial z}-\frac{v\cos\psi}{h}\Big)\tilde{v}\Big\}+$$

$$\frac{\lambda}{Rh}\Big\{xu\tilde{u}\sin^2\psi+2hu\tilde{u}\sin\psi+xu\sin\psi\frac{\partial\tilde{u}}{\partial x}+xu\sin\psi\frac{\partial\tilde{v}}{\partial\theta}$$

$$+xu\tilde{w}\sin\psi\cos\psi+R^{-\frac{1}{2}}w\tilde{u}\sin\psi\cos\psi+R^{-\frac{1}{2}}h\tilde{u}\sin\psi\frac{\partial w}{\partial z}+xuh\sin\psi\frac{\partial\tilde{w}}{\partial z}$$

$$+hu\frac{\partial\tilde{u}}{\partial x}+hu\frac{\partial\tilde{v}}{\partial\theta}+uh\tilde{w}\cos\psi+uh^2\frac{\partial\tilde{w}}{\partial z}+R^{-\frac{1}{2}}w\cos\psi\frac{\partial\tilde{u}}{\partial x}+R^{-\frac{1}{2}}h\frac{\partial w}{\partial z}\frac{\partial\tilde{u}}{\partial x}$$

$$+R^{-\frac{1}{2}}w\cos\psi\frac{\partial\tilde{v}}{\partial\theta}+R^{-\frac{1}{2}}h\frac{\partial w}{\partial z}\frac{\partial\tilde{v}}{\partial\theta}+R^{-\frac{1}{2}}w\tilde{w}\cos^2\psi+R^{-\frac{1}{2}}h\tilde{w}\cos\psi\frac{\partial w}{\partial z}$$

$$+R^{-\frac{1}{2}}wh\cos\psi\frac{\partial\tilde{w}}{\partial z}+R^{-\frac{1}{2}}h^2\frac{\partial w}{\partial z}\frac{\partial\tilde{w}}{\partial z}\Big\}.$$

References

ABRAMOWITZ, M & STEGUN, I.A. 1964 A handbook of mathematical functions. Frankfurt: National Bureau of Statisitics.

APPELQUIST, E. 2014 Direct numerical simulations of the rotating-disk boundary-layer flow. Licentiate thesis, Royal Institute of Technology, KTH Mechanics, ISBN: 978-91-7595-202-4

COOPER, A.J., HARRIS, J.H., GARRETT, S.J., THOMAS, P.J. & ÖZKAN, M. 2015 The effect of anisotropic and isotropic roughness on the convective stability of the rotating disk boundary layer, *Phys. Fluids*, **27**, 014107.

GARRETT, S. J. & PEAKE, N. 2007 The absolute instability of the boundary layer on a rotating cone *European. J. Mech. B.* **26**, 344–53.

GARRETT, S. J., HUSSAIN, Z. & STEPHEN, S. O. 2009 The crossflow instability of the boundary layer on a rotating cone. *J. Fluid Mech.* **622**, 209–232.

GREGORY, N., STUART, J.T. & WALKER, W.S. 1955 On the stability of three-dimensional boundary layers with applications to the flow due to a rotating disk. *Philos. Trans. R. Soc. London Ser. A.* **248**, 155–199.

GREGORY, N. & WALKER, W.S. 1960 Experiments on the effect of suction on the flow due to a rotating disk. *Phil. Trans. R. Soc. Lond.*, **248**, 225–234.

GRIFFITHS 2015 Flow of a generalised Newtonian fluid due to a rotating disk. *J. Non-Newt Fluid*, **221**, 9–17.

HALL, P. 1986 An investigation of the stationary modes of instability of the boundary layer on a rotating disk. *Proc. Roy. Soc. London Ser. A.*, 406, 93–106.

HUSSAIN, Z. 2009 Stability and transition of three dimensional rotating boundary layers. PhD Thesis, University of Birmingham.

HUSSAIN, Z., GARRETT, S.J. & STEPHEN, S.O. 2014 The centrifugal instability of the boundary-layer flow over slender rotating cones', *J. Fluid Mech.* **775**, 275–293.

HUSSAIN, Z., GARRETT, S.J., STEPHEN, S.O. & GRIFFITHS, P.T. 2015 The centrifugal instability of the boundary-layer flow over a slender rotating cone in an enforced axial free-stream, to appear in *J. Fluid. Mech.*

IMAYAMA, S., ALFREDSSON, P.H. & LINGWOOD, R.J. 2013 An experimental study of edge effects on rotating-disk transition. *J. Fluid Mech.*, **716**, 638–657.

ITOH, N. 1994 Instability of three-dimensional boundary layers due to the streamline curvature. *Fluid Dyn. Res.* **14**, 353–366.

ITOH, N. 1996 Simple cases of the stream-line curvature instability in three-dimensional boundary layers. *J. Fluid Mech.* **317**, 129–154.

KAPPESSER, R., GREIF, R. & CORNET, I. 1973 Mass transfer on rotating cones. *Appl. Sci. Res.* **28**, 442–52.

KOBAYASHI, R. 1981 Linear stability theory of boundary layer along a cone rotating in axial flow. *Bull. Japan Soc. Mech. Engrs.* **24**, 934–940.

KOBAYASHI, R., KOHAMA, Y. & KUROSAWA, M. 1983 Boundary-layer transition on a rotating cone in axial flow. *J. Fluid Mech.* **127**, 341–52.

KOBAYASHI, R. & IZUMI, H. 1983 Boundary-layer transition on a rotating cone in still fluid. *J. Fluid Mech.* **127**, 353–64.

LINGWOOD, R. J. 1995 Absolute instability of the boundary layer on a rotating disk. *J. Fluid Mech.* **299**, 17–33.

LINGWOOD, R. J. 1996 An experimental study of absolute instability of the rotating-disk boundary layer flow. *J. Fluid Mech.* **314**, 373–405.

MALIK, M. R. 1986 The neutral curve for stationary disturbances in rotating-disk flow. *J. Fluid Mech.* **164**, 275–87.

RILEY, N. 1964 The heat transfer from a rotating disk. *Q. J. Mech. Appl. Math.* **17**, 331–349.

SEDDOUGUI, S.O. 1990 A nonlinear investigation of the stability modes of instability of the three-dimensional compressible boundary layer due to a rotating disc, *Q. Jl Mech. appl. Math.* 43, Pt. 4.

SMITH, F.T 1979 Non-parallel flow stability of the Blasius boundary layer. *Proc. Royal Soc. A* **43**, 91–109.

STEWARTSON, K. 1964 The theory of laminar boundary layers in compressible fluids. Oxford University Press.

TOWERS, P.D. & GARRETT, S.J. 2012 On the stability of the compressible boundary-layer flow over a rotating cone, *Proceedings of the 42nd AIAA Fluid Dynamics Conference*, New Orleans, LA, USA.

TOWERS, P.D. & GARRETT, S.J. 2014 Similarity solutions of compressible flow over a rotating cone with surface suction, *Thermal Science*, doi:10.2298/TSCI130408032T

TOWERS, P.D. 2013 The stability and transition of the compressible boundary-layer flow over broad rotating cones, PhD Thesis, University of Leicester.

TURKYILMAZOGLU, M., COLE, J. W. & GAJJAR, J. S. B. 2000 Absolute and convective instabilities in the compressible boundary layer on a rotating disk. *Theor. Comput. Fluid Dyn.* **14**, 21–37.

TURKYILMAZOGLU, M. & UYGUN, N. 2004 Basic compressible flow over a rotating disk. *Hace. J. Math. Stat.* **33**, 1–10.

TURKYILMAZOGLU, M. 2005 Lower branch modes of the compressible boundary layer flow due to a rotating disk. *Stud. Appl. Math.* **114**, 17–43.

TURKYILMAZOGLU, M. 2007 Influence of finite amplitude disturbances on the nonstationary modes of a compressible boundary layer flow. *Stud. Appl. Math.* **118**, 199–220.